

# Conformational switching of the 26S proteasome enables substrate degradation

Mary E Matyskiela<sup>1</sup>, Gabriel C Lander<sup>2,4</sup> & Andreas Martin<sup>1,3</sup>

**The 26S proteasome is the major eukaryotic ATP-dependent protease, responsible for regulating the proteome through degradation of ubiquitin-tagged substrates. Its regulatory particle, containing the heterohexameric AAA+ ATPase motor and the essential deubiquitinase Rpn11, recognizes substrates, removes their ubiquitin chains and translocates them into the associated peptidase after unfolding, but detailed mechanisms remain unknown. Here we present the 26S proteasome structure from *Saccharomyces cerevisiae* during substrate degradation, showing that the regulatory particle switches from a preengaged to a translocation-competent conformation. This conformation is characterized by a rearranged ATPase ring with uniform subunit interfaces, a widened central channel coaxially aligned with the peptidase and a spiral orientation of pore loops that suggests a rapid progression of ATP-hydrolysis events around the ring. Notably, Rpn11 moves from an occluded position to directly above the central pore, thus facilitating substrate deubiquitination concomitant with translocation.**

The ubiquitin-proteasome system is responsible for rapid degradation of critical regulatory proteins as well as proteome quality control and homeostasis in all eukaryotic cells<sup>1</sup>. Substrates selected for degradation are covalently marked with chains of the small protein ubiquitin, which targets them to the 26S proteasome for subsequent proteolysis. Although recent studies have illuminated the overall architecture of this ATP-dependent protease, the structural and molecular mechanisms of substrate engagement and translocation remain poorly understood. Indeed, little is known in general about the detailed mechanisms of protein unfoldases in the family of ATPases associated with various cellular activities (AAA+), despite the broad importance of ATP-dependent protein unfolding, remodeling and degradation in the cell<sup>2</sup>.

The 26S proteasome is a massive molecular machine with at least 34 different subunits forming a barrel-shaped 20S peptidase capped on one or both ends by a 19S regulatory particle<sup>3</sup>. The proteolytic active sites of the peptidase are sequestered in an internal chamber, which protein substrates can access only after unfolding, deubiquitination and translocation by the regulatory particle<sup>4–6</sup>. This regulatory particle consists of 20 subunits and can be divided into two stably associated subcomplexes: the lid and the base<sup>7</sup>.

The base subcomplex contains the proteasomal molecular motor, a heterohexameric ring of six distinct AAA+ ATPase subunits in the order Rpt1, Rpt2, Rpt6, Rpt3, Rpt4 and Rpt5 (refs. 8,9). In addition, it includes two large scaffolding proteins (Rpn1 and Rpn2), the ubiquitin receptor Rpn13 (ref. 10) and the nonessential deubiquitinating enzyme (DUB) Ubp6 (ref. 11). The AAA+ domains of the ATPase subunits are predicted to contact the substrate through conserved

loops in the central pore and to use the energy of ATP binding and hydrolysis to undergo conformational changes and exert a mechanical pulling force that unfolds and translocates the substrate into the peptidase<sup>12–16</sup>. Each ATPase subunit also contains an N-terminal domain, which is composed of an oligomer-binding (OB) fold and an N-terminal helix<sup>17</sup>. Together, the six OB folds of the ATPase hexamer form a separate ring (the N ring) above the AAA+ domains, and the N-terminal helices pair into three coiled coils that protrude from this N ring. Distinct tails at the C termini of the ATPase subunits mediate attachment of the base to the 20S peptidase through interactions with dedicated pockets on the peptidase surface<sup>18,19</sup>. Previous structural studies have shown that these two subcomplexes bind in an asymmetric fashion, with the pores of the AAA+ and N-ring unexpectedly offset from a coaxial alignment with the peptidase<sup>20–22</sup>.

The lid subcomplex is laterally bound to the holoenzyme, partially surrounding the base and also contacting the 20S peptidase<sup>20</sup>. Six of the lid subunits (Rpn3, Rpn5, Rpn6, Rpn7, Rpn9 and Rpn12) interact through C-terminal proteasome-CSN-eIF3 (PCI) domains in a horseshoe-shaped arrangement, with their N-terminal domains extending radially outward<sup>20,23</sup>. The intrinsic ubiquitin receptor Rpn10 binds the periphery of the proteasome at the far end of Rpn9's N-terminal domain. Rpn8 and the essential DUB Rpn11 (ref. 24) form a dimer that projects toward the center of the regulatory particle<sup>25</sup>, thus positioning Rpn11 near the N ring. This DUB has been shown to remove entire ubiquitin chains from the substrate by cleaving the isopeptide bond of the proximal ubiquitin moiety<sup>26</sup>. Notably, Rpn11's deubiquitination activity was found to depend on ATP hydrolysis by the proteasome, suggesting a potential coupling

<sup>1</sup>Department of Molecular and Cell Biology, University of California, Berkeley, Berkeley, California, USA. <sup>2</sup>Life Sciences Division, Lawrence Berkeley National Laboratory, University of California, Berkeley, Berkeley, California, USA. <sup>3</sup>California Institute for Quantitative Biosciences, University of California, Berkeley, Berkeley, California, USA. <sup>4</sup>Present address: Scripps Research Institute, La Jolla, California, USA. Correspondence should be addressed to G.C.L. (glander@scripps.edu) or A.M. (a.martin@berkeley.edu).

Received 26 April; accepted 14 May; published online 16 June 2013; doi:10.1038/nsmb.2616

**Figure 1** Conformational transition of the proteasome from a substrate-free to an actively degrading state. The structures of wild-type proteasome in its substrate-free (left) and substrate-engaged state (right) identically oriented on the basis of their 20S peptidase (gray), with a dashed line indicating the central axis of the peptidase pore. Substrate engagement induces a conformational rearrangement of the regulatory particle, including a rotation of Rpn2 (dark blue), Rpn13 (light orange) and the lid subcomplex (yellow), the formation of contacts between the ubiquitin receptor Rpn10 (magenta) and the Rpt4–Rpt5 coiled coil, and a coaxial alignment of the N ring and the AAA+ ring (both cyan) with the peptidase. Furthermore, the DUB Rpn11 (green) shifts to a central location, occluding the processing pore. The extra density (red) observed in the reconstruction of the degrading proteasome is attributed to a globular domain of the substrate.

with substrate translocation<sup>24</sup>. However, the mechanism for this coupling remains unknown.

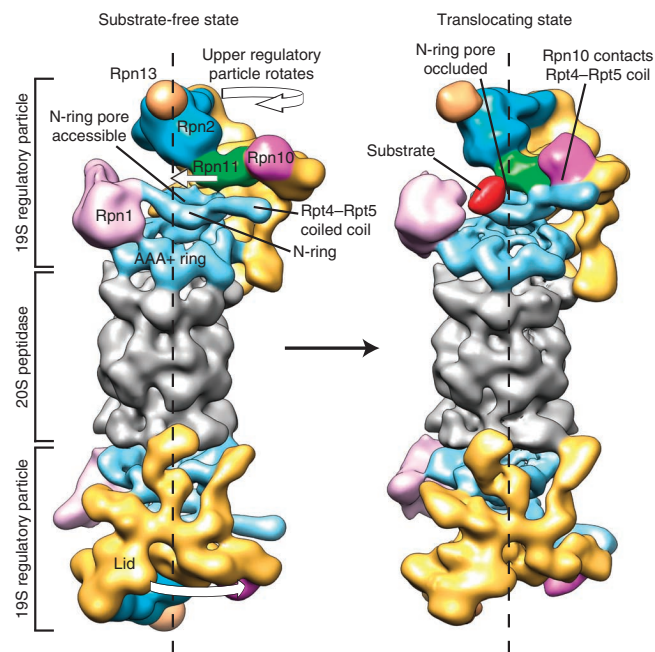
Previous crystallographic studies of several related RecA-type and AAA+ helicases revealed that their AAA+ domains and pore loops deviate from a planar organization and exhibit staircase arrangements around the hexameric ring<sup>27–29</sup>. On the basis of current mechanistic models for these motors, individual AAA+ domains are predicted to continually progress through the distinct conformational registers of the staircase as they hydrolyze ATP<sup>27</sup>. Accordingly, within an ensemble of hydrolyzing proteasome particles, the heterohexameric ATPase ring would be expected to display a variety of distinct conformational states. However, previous EM reconstructions of the proteasome in the presence of saturating ATP show that the ATPase domains adopt a fixed spiral-staircase arrangement, with Rpt3 in the highest and Rpt2 in the lowest position for every complex<sup>20,25</sup>. The fixed organization of the proteasomal ATPases thus contradicts the currently predicted mechanisms for AAA+ unfoldases, and this suggests that either the observed staircase reflects a translocation-incompetent state or substrate translocation functions by an alternative mechanism. Distinguishing between these scenarios has thus far been impossible, owing to the lack of structural information on the proteasome or any other protein unfoldase during substrate degradation.

To gain structural insights into the mechanisms of substrate processing by the 26S proteasome, we solved the cryo-EM structure of the holoenzyme during the degradation of a ubiquitin-tagged substrate. We identified an alternative, translocation-competent conformation of the regulatory particle, characterized by a repositioned Rpn11 and a rearranged ATPase ring that together enable efficient substrate degradation.

## RESULTS

### Structure of substrate-bound proteasome

We first solved the cryo-EM structure of wild-type holoenzyme during degradation of a ubiquitinated substrate. Occupancy was maximized by incubating the proteasome with an excess of a previously characterized model substrate<sup>20</sup> consisting of GFP fused to a destabilized titin I27 domain and an unstructured 111-amino acid segment for engagement<sup>30,31</sup>. Two-dimensional analysis revealed that the regulatory particles of these actively degrading proteasomes were much more variable than those of previously observed ATP-bound, substrate-free (apo) proteasomes (**Supplementary Fig. 1a–c**). Three-dimensional analyses showed that a large fraction of the regulatory particles had undergone a marked rearrangement, which included a blockage of the N-ring pore by Rpn11 as well as the formation of contacts between Rpn10 and the Rpt4–Rpt5 coiled coil (**Fig. 1** and **Supplementary Fig. 1d**). Notably, the regulatory particles in this altered conformation displayed an additional low-resolution electron



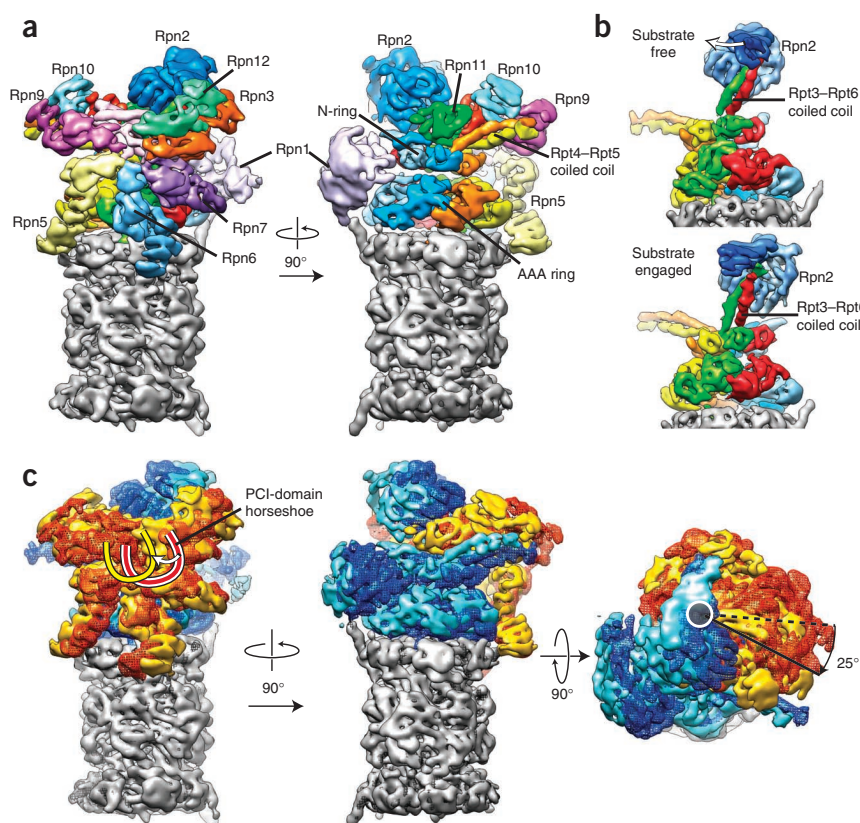
density near the N ring and Rpn11, consistent with a flexibly attached globular structure. GFP exhibits a high thermodynamic stability and fast refolding kinetics<sup>32</sup> and may have numerous ubiquitin chains attached to its many surface-exposed lysine residues. Because of these obstacles, GFP processing may represent the rate-limiting step in the degradation of this substrate, causing an accumulation of proteasome particles that have translocated the fusion construct up to the GFP moiety. This would suggest that the observed additional density arises from folded GFP at the entrance to the N ring (**Fig. 1** and **Supplementary Fig. 1e**).

Within the ensemble of doubly capped proteasomes, we observed three different populations of holoenzyme: 25% showed both regulatory particles in the substrate-engaged conformation, 35% had both regulatory particles in the apo conformation with no indication of additional density, and 40% were asymmetric with one apo and one substrate-engaged regulatory particle. That we observe this distribution of asymmetric as well as dually translocating proteasomes indicates that there is neither positive nor negative cooperativity between the two regulatory particles of the holoenzyme. Substrate degradation can thus also occur simultaneously from both ends, a phenomenon that had been unexpected on the basis of previous studies of other AAA+ proteases<sup>33</sup>.

To achieve a higher-resolution structure of the regulatory particle in the translocating conformation, it was necessary to trap a uniform ensemble of substrate-engaged proteasome particles. We therefore purified yeast 26S holoenzymes containing an Rpn11 active site mutation (AXA<sup>24,34</sup>; **Supplementary Fig. 2a**) that abolishes deubiquitination. This mutation prevents further substrate processing when the uncleaved ubiquitin chain arrives at the entrance to the unfoldase pore<sup>24,26</sup>. To additionally increase sample homogeneity, we deleted Rpn13, making Rpn10 the sole intrinsic ubiquitin receptor for substrate recruitment. Notably, this mutant enzyme exhibits wild-type levels of basal ATP hydrolysis, which are stimulated by the presence of a ubiquitinated substrate (**Supplementary Fig. 2b**). By solving a high-resolution cryo-EM structure, we confirmed that the structural organization of this mutant enzyme in the absence of substrate was indistinguishable from that of the wild-type holoenzyme, except for the lack of Rpn13 (**Supplementary Fig. 3a**).

**Figure 2** The subnanometer-resolution structure of the substrate-engaged 26S proteasome.

(a) The segmented cryo-EM reconstruction of the substrate-engaged proteasome (Rpn11<sup>AXA</sup> Rpn13Δ), with the regulatory particle colored by subunit and the peptidase in gray. (b) Side views of the base subcomplex in the substrate-free (top) and substrate-bound state (bottom), emphasizing the substrate-induced twisting of the Rpt3–Rpt6 coiled coil (green and red) that results in a rotation of Rpn2 (blue). The core-particle densities were aligned for this comparison. (c) Motions associated with substrate engagement, depicted by overlay of the substrate-free and substrate-bound structures that are aligned by their 20S peptidases. The base (blue mesh, apo; solid cyan, substrate bound) and the lid (red mesh, apo; solid yellow, substrate bound) undergo large rotations and shifts, whereas the peptidase (black mesh, apo; solid gray, substrate bound) does not exhibit notable differences. Left, the red and yellow curved lines illustrate the movement of the horseshoe-shaped arrangement of PCI domains from its substrate-free to substrate-bound position, respectively. Right, top view illustrating the 25° rotation of the upper regulatory particle around the axis of the Rpt3–Rpt6 coiled coil (black circle).



For the substrate-bound structure of the mutant proteasome, we reduced the background around imaged particles by using a simplified substrate (**Supplementary Fig. 3c**) containing a 52-amino acid flexible tail at the C terminus, a small globular domain (N1 domain of the gene-3-protein, G3P) and a single lysine at the N terminus that allowed for homogeneous ubiquitination. Wild-type proteasome efficiently degrades this substrate in a C- to N-terminal direction at a rate of ~1 per minute per enzyme (**Supplementary Fig. 4a**), whereas the Rpn11<sup>AXA</sup> Rpn13Δ mutant proceeds through the globular domain and stalls when the N-terminally attached ubiquitin chain reaches the entrance to the pore. We therefore do not expect to observe electron density for the globular domain of the substrate. However, the presence of stalled substrate on the mutant proteasome was confirmed by pulldown experiments (**Supplementary Fig. 4b**).

### Rearrangement of the regulatory particle

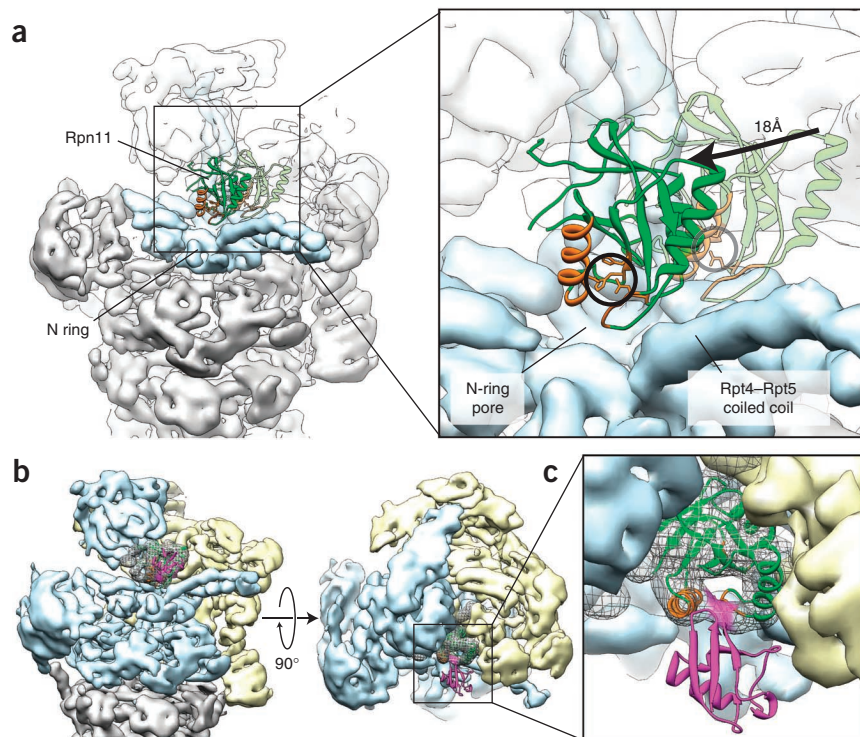
Our subnanometer-resolution cryo-EM reconstruction reveals that substrate induces broad changes in the structure of the regulatory particle (**Fig. 2a** and **Supplementary Figs. 3b** and **5a–c**) leading to a coaxial alignment of the DUB Rpn11, the N ring, the AAA+ ring and the entrance to the peptidase (**Supplementary Movie 1**). The N ring is shifted and tilted by 16 Å and 13°, respectively, and this movement is further propagated to the upper part of the regulatory particle through the N-terminal coiled coil of Rpt3 and Rpt6 (**Fig. 2b**). This coiled coil suspends Rpn2 above the unfoldase<sup>20</sup>, and the change in position of the N ring causes it to twist and hence causes Rpn2 to rotate. Because Rpn2 forms static interactions with the lid subunits Rpn3, Rpn11 and Rpn12 as well as with the bundle of lid-subunit C termini<sup>25</sup>, the movement of Rpn2 translates into a 25° rotation of the lid around the Rpt3–Rpt6 coiled coil anchor point (**Fig. 2c**). Excluded from this rotation are the N-terminal domains of Rpn5 and Rpn6, which contact the AAA+ ring and the core peptidase and therefore perform distinct motions to accommodate the reorganization of

subcomplexes. Although we examined the 20S peptidase in detail, we did not observe any interpretable changes in the density of this subcomplex (**Supplementary Fig. 3b**).

To eliminate the possibility that this new conformation is an alternative apo state, we searched the data sets of substrate-free proteasome particles for this conformer. In fact, we did observe particles in this new conformation, but there was a strict correlation with the presence of additional density at the entrance of the pore, in a location similar to that of the previously observed density for the GFP model substrate (**Supplementary Fig. 5d**). It is therefore likely that this additional density results from endogenous substrates that co-purify with proteasomes from yeast, and we were able to confirm the presence of these ubiquitinated proteins in our proteasome preparations by anti-ubiquitin western blotting (**Supplementary Fig. 5e**). Together, these findings indicate that the new conformation is not simply an alternative apo state but a previously undescribed degradation mode that is induced by substrate.

We did not observe density for the unstructured polypeptide in the central pore, which is not surprising given the probable heterogeneity in its orientation in the pore and the limited resolution of the EM reconstruction. However, we used cross-linking and partial-degradation experiments to confirm that the substrate polypeptide is indeed translocated through the central pore (**Supplementary Fig. 6a,b**). We therefore propose that the observed conformational switch originates from interactions between substrate and the AAA+ domains of Rpt1–Rpt6. Unfoldases of the AAA+ family are known to respond to substrate engagement with an increase in ATPase activity<sup>35–37</sup>, potentially owing to better subunit coordination in an altered ring conformation (base reorganization described below). ATP hydrolysis could thus be used to drive the conformational switch of the regulatory particle into a degradation-competent state after the substrate contacts ATPase subunits in the central pore. Ubiquitin

**Figure 3** Rpn11 is coaxially aligned with the ATPase pore in the substrate-engaged state. **(a)** Atomic model of the DUB Rpn11 (PDB 4B4T) is used to show the substrate-induced movement of this subunit relative to the N ring. In the substrate-free state, Rpn11 (semitransparent green ribbon), with the residues predicted to form the catalytic groove<sup>42</sup> highlighted in orange, is situated to the side of the N ring and behind the Rpt4–Rpt5 coiled coil. Conformational changes in the regulatory particle shift Rpn11 to a position directly above the N-ring pore in the substrate-bound state (opaque ribbon). **(b)** The expected orientation of a ubiquitin moiety (magenta ribbon)<sup>42</sup> with its C terminus bound in the Rpn11 catalytic groove (green mesh, Rpn11 electron density; green ribbon, atomic model; orange, catalytic groove) is shown from a side and top view. **(c)** Close-up of the modeled interactions between ubiquitin and Rpn11 from the top view. The continuous density closing the catalytic groove (magenta mesh) may correspond to the C terminus of ubiquitin.



binding to the only receptor on our mutant proteasome, Rpn10, is unlikely to induce the conformational switch because its ubiquitin-interacting motif (UIM) is flexibly attached and, in contrast to its globular domain, is unresolved even in the substrate-bound state. If ubiquitin binding triggered the switch to the observed conformation, it would in fact hinder substrate engagement because access to the N-ring pore becomes considerably restricted by Rpn11 (Fig. 1). Furthermore, there are several examples for efficient ubiquitin-independent protein degradation by the proteasome<sup>38–41</sup>. Thus, for the ubiquitin-dependent majority of proteasome substrates, ubiquitin binding seems to be required for efficient engagement primarily because it increases the local substrate concentration at the proteasome surface and maximizes the probability that a flexible segment enters the processing pore.

### Repositioning of Rpn11

In the substrate-free conformation of the regulatory particle, Rpn11 is located to the side of the N-ring pore. Docking the crystal structure of a related DUB, AMSH-LP<sup>42</sup>, into this structure revealed that the Rpn11 catalytic groove is positioned directly above the bottom portion of the N-terminal coiled coil of Rpt4 and Rpt5 (ref. 20) (Fig. 3a), and this may prevent a substrate-bound ubiquitin from reaching the DUB active site. Notably, however, in this preengaged state the N-ring pore is accessible to the flexible tail of an incoming substrate that is tethered to a ubiquitin receptor.

Upon substrate engagement by the AAA+ ring, Rpn11 shifts by 18 Å toward the center of the regulatory particle, so that it is placed directly above the N-ring pore, and its active site is liberated for ubiquitin cleavage (Fig. 3a and Supplementary Movie 1). This large movement of Rpn11 may explain the previously described translocation dependence of deubiquitination<sup>24</sup>, and it offers a mechanism to prevent the premature removal of ubiquitin from a substrate that is not yet engaged.

In the substrate-engaged conformation, the catalytic groove of Rpn11 is aligned with the axis of the unfoldase pore, and a ubiquitin moiety bound with its C-terminal tail in this groove would be positioned alongside Rpn11, where it would have no steric clashes or interactions with other subunits of the regulatory particle (Fig. 3b).

This lack of interactions may explain the absence of observable electron density for the Rpn11-bound ubiquitin moiety, as its globular domain can adopt a wide range of orientations. However, we did observe a continuum of EM density across the catalytic groove (Fig. 3c and Supplementary Fig. 7a). On the basis of the crystal structure of ubiquitin-bound AMSH-LP<sup>42</sup>, and given that the tertiary organization of Rpn11 does not change upon substrate engagement (Supplementary Fig. 7b,c), the additional bridging density may correspond to a short three-stranded  $\beta$ -sheet formed between Rpn11 and the C-terminal tail of ubiquitin. Besides this defined interaction with Rpn11, the ubiquitin chain appears to make no additional rigid contacts with other proteasome subunits. Even the receptor UIM of Rpn10 is unresolved in EM reconstructions, owing to its flexible attachment, which explains the lack density for a ubiquitin chain bound to it.

The placement of Rpn11 above the N ring positions its active site only  $\sim 10$  Å from the pore entrance, such that the isopeptide branch-point of a substrate-attached ubiquitin must pass by the catalytic groove *en route* to the central pore. Rpn11 may thus act as a gatekeeper, scanning the substrate polypeptide to ensure that all ubiquitins are removed before reaching and obstructing the entrance to the pore. In addition, the location of the Rpn11 active site probably determines its specificity for cleaving the proximal ubiquitin<sup>26</sup> because endoisopeptidase activity would require the positioning of a second ubiquitin below Rpn11, in a region that is sterically occluded by the N ring (Fig. 3b).

### Translocation-competent state of the base

Our EM structure reveals that substrate engagement in the central pore triggers major changes in the conformation of the AAA+ ring, primarily by inducing the subunits to shift and rotate away from the lid (Supplementary Movie 1). This movement of subunits leads to a global shift of the AAA+ ring relative to the peptidase, from a 10-Å offset to a nearly perfect coaxial alignment (Fig. 4a,b). Despite this transition, the C-terminal tails of Rpt2, Rpt3 and Rpt5, which contain the conserved hydrophobic-tyrosine-unspecified residue (HbYX)

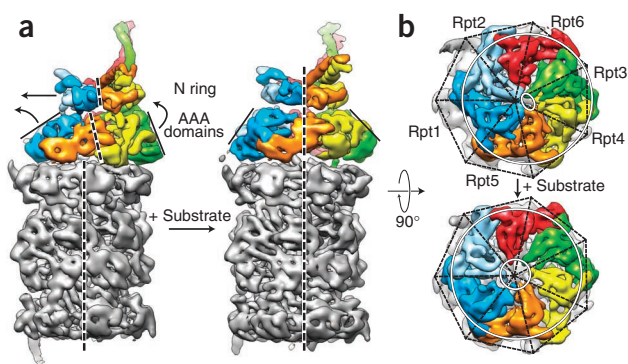


**Figure 4** Substrate-induced rearrangement of the ATPase subunits creates a widened pore and a continuous central channel throughout the enzyme. **(a)** The segmented electron densities corresponding to the ATPase subunits Rpt1–Rpt6 (rainbow) and the peptidase (gray) are shown for the proteasome in the absence (left) and presence (right) of substrate, with dashed lines indicating the axes of the central channels. Substrate engagement causes the AAA+ domains of the Rpts to individually rotate and shift into a more symmetric and coaxially aligned ring. The N ring also tilts and shifts, and together these changes result in the formation of a continuous channel through the ATPases to the peptidase. **(b)** The peptidase (gray) and the AAA+ domains of the ATPases (rainbow) are shown from above in the absence (top) and presence (bottom) of substrate, with dashed black lines indicating the seven-fold symmetry of the peptidase below. The large white circles encompassing the AAA+ domains emphasize the degree of alignment between the AAA+ ring and the peptidase. The smaller white circles depict the ATPase-pore diameters for the two states.

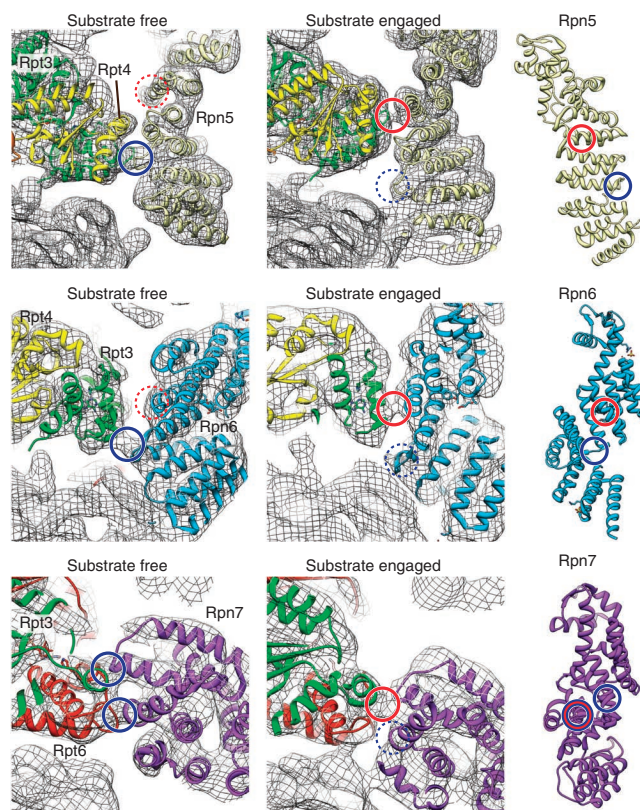
motif for peptidase interaction, remain docked in their respective binding pockets (**Supplementary Fig. 8a**). Notably, the Rpt motions result in an approximately four-fold widening of the central pore, from an almost closed state to an open state that can readily accommodate a translocating polypeptide (**Fig. 4b**). The pore diameter in both the preengaged and substrate-bound conformation is actually smaller than it appears in our structures because heterogeneity in the position of pore loops causes some lack of density in the central channel. In addition to the motions of the AAA+-domain hexamer, the rigid N ring also shifts to become aligned with the peptidase, thus creating a continuous channel through the entire complex (**Fig. 4a**). Together, this coaxial alignment and the expansion of the central pore most probably facilitate efficient substrate translocation (**Supplementary Fig. 8b**).

The lid subcomplex appears to have an important role in stabilizing the reorganized architecture of the base. We observe three major interactions between the lid and the base in both the substrate-free and substrate-bound reconstructions. The small AAA+ subdomain of Rpt3 contacts the lid subunits Rpn5 and Rpn6 while the Rpt3–Rpt6 AAA+ interface interacts with Rpn7 (**Fig. 5**). During the substrate-induced conformational transition, Rpn7 remains in contact with the Rpt3–Rpt6 interface and thus may function as a joint to accommodate the differential movements of the lid and base subcomplexes. In contrast, the base movements cause Rpt3 to switch its contacts with Rpn5 and Rpn6 to new binding sites that are located 30 and 25 Å farther toward the respective PCI domains. Thus we define

two distinct modes of interaction between the lid and the base that stabilize the ATPase ring in either its preengaged state or in a translocation-competent conformation that is maintained throughout substrate processing.

An important consequence of the substrate-induced rotation of Rpt subunits is that the interfaces between the AAA+ domains become highly uniform around the ring (**Fig. 6a**). These uniform interfaces are reminiscent of the ‘rigid bodies’ that are formed in the homohexameric unfoldase ClpX between each large AAA+ subdomain and the small subdomain of the neighboring subunit<sup>43</sup>. On the basis of rigidifying intersubunit cross-linking of the ClpX hexamer, it has been proposed that ATP hydrolysis changes the relative orientation of the large and small AAA+ subdomains within a given subunit and thus drives movements of the rigid body formed with the subdomain of the neighbor to propel a substrate polypeptide through the central pore<sup>43,44</sup>. The apparent formation of uniform intersubunit contacts in the proteasomal Rpt ring upon substrate engagement therefore suggests the transition from a preengaged to a more symmetrical

**Figure 5** Bimodal stabilization of the preengaged or translocation-competent base conformation by the lid. Close-up view of the lid-base interface, highlighting alternative contacts between Rpt and Rpn subunits in the substrate-free and substrate-engaged conformations of the regulatory particle. The positions of Rpt3 (green), Rpt4 (yellow) and Rpt6 (red) within the substrate-free and substrate-engaged EM densities (gray mesh) are shown by fitted crystal structures of the homologous PAN AAA+ domain (PDB 3H4M). The crystal structure of Rpn6 (cyan, PDB 3TXN<sup>49</sup>) and homology models of Rpn5 (PDB 4B4T, light yellow) and Rpn7 (PDB 4B4T, purple)<sup>25</sup> are shown on the right and docked into their corresponding positions in the EM density (middle and left). Both Rpn5 and Rpn6 interact with the small AAA+ subdomain of Rpt3, while Rpn7 contacts the interface between the small AAA+ subdomain of Rpt6 and the large AAA+ subdomain of Rpt3. These interactions in the substrate-free state are highlighted with solid blue circles. The substrate-engaged reconstruction reveals that Rpt3 switches its contacts with Rpn5 and Rpn6 to new binding sites (solid red circles) that are located 30 and 25 Å farther toward the respective PCI domains. In contrast, Rpn7 remains in contact with the Rpt6–Rpt3 interface but reduces its interaction points from two (blue circles) to one (red circle). This semistatic joint with Rpn7 may function as a pivot point in switching from a substrate-free to a substrate-bound conformation of the regulatory particle. Dashed circles indicate the corresponding contacts in the alternative conformation.



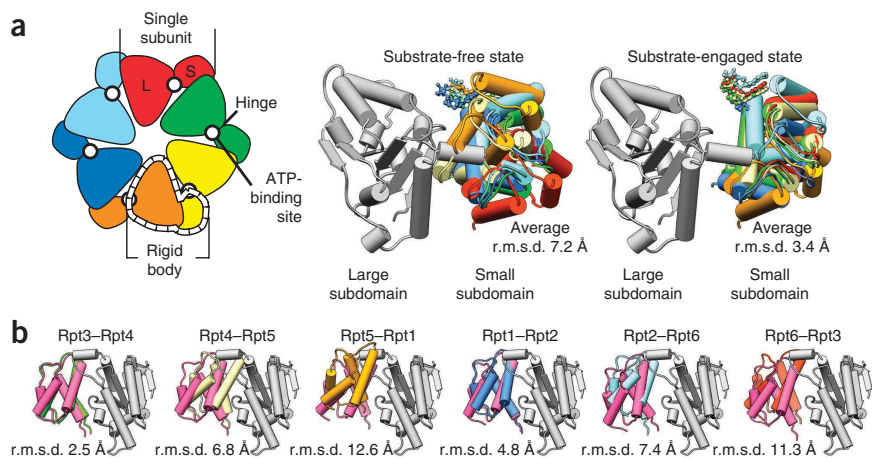


**Figure 6** The translocation-competent conformation of the base exhibits uniform AAA+ domain interfaces. **(a)** Left, cartoon with subunits individually colored, delineating the intersubunit rigid body (dashed line) formed from a small AAA+ subdomain and the large AAA+ subdomain of its counterclockwise neighbor<sup>43,44</sup>. The six rigid bodies derived from docked crystal structures of individual large and small AAA+ subdomains of the homologous PAN (PDB 3H4M) were superimposed by aligning the large subdomains. Substrate engagement induces uniform interfaces between subdomains of neighboring subunits, reflected by a lower average r.m.s. deviation of the small subdomains. **(b)** Rigid bodies formed between large and small AAA+ subdomains at each Rpt interface in the absence and presence of substrate, superimposed and aligned by their large subdomain (gray). The small AAA+ domains are shown individually colored in the substrate-free state and magenta in the bound state.

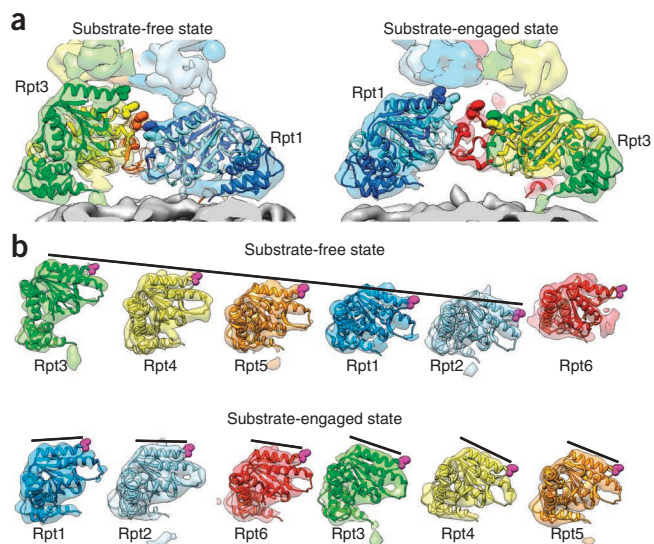
translocation-competent state that allows optimal coordination between ATPase subunits. Notably, one of the interfaces, between the small AAA+ subdomain of Rpt3 and the large AAA+ subdomain of Rpt4 (Fig. 6b), already exhibits this rigid-body orientation in the substrate-free state of the AAA+ ring. Rpt3 and Rpt4 are located at the top of the spiral staircase adopted by the Rpts before substrate engagement and would therefore be the first subunits to interact with an incoming substrate<sup>20</sup>. Substrate-induced movement of their stably associated large and small AAA+ subdomain may propagate the formation of uniform interfaces to the remainder of the Rpts and thus induce the transition to a translocation-competent ring conformation that is then maintained until the substrate has been completely translocated.

Notably, as the Rpt-ring conformation changes in response to substrate engagement, each AAA+ subunit rotates to a variable degree. This results in a switch from the pronounced spiral staircase of subunits in the substrate-free state to a nearly planar ring when substrate is engaged (Fig. 7 and Supplementary Movie 1). The strong pitch of the spiral in the absence of substrate originates from the large AAA+ subdomains of

**Figure 7** Rearrangement of the spiral staircase upon substrate engagement. **(a)** Cutaway side view of the Rpt ring in the substrate-free (left) and substrate-engaged (right) state, with Rpt6 and Rpt5 removed for clarity, respectively, and oriented with the top subunit of each spiral staircase on the left. Individually docked copies of the PAN crystal structure (ribbons, PDB 3H4M) reveal different spiral-staircase arrangements in the two states, emphasized by a sphere representation of the pore-loop residue that is predicted to drive translocation. **(b)** AAA+ domains of Rpt1–Rpt6, shown individually in the same orientation, with their pore loops facing right and the aromatic pore-loop residue shown (magenta). In the absence of substrate, the entire AAA+ domains are rotated to varying degrees away from the central pore, thus leading to a pronounced spiral-staircase arrangement of large subdomains with a global pitch that is indicated by a continuous line. Substrate engagement arranges the AAA+ domains at a more uniform height, with a lower-pitch spiral staircase of pore loops established solely through varied tilting of the large subdomains (black lines).

Rpt1–Rpt6 being arranged at different heights along the central pore axis, with Rpt3 at the top and Rpt2 at the bottom position<sup>20,25</sup>. In contrast, the large AAA+ subdomains in the substrate-engaged conformation are at one level, but each is tilted to different degrees about an axis lying in the plane of the ring (Fig. 7). This variable tilting results in a new spiral arrangement of the pore loops, with Rpt1 now assuming the uppermost position and Rpt4 the bottom. Despite their structural differences, both ring conformations contain a bridging subunit that connects the top and bottom of the spiral. Rpt6 and Rpt5 fill this intermediate position in the substrate-free and substrate-bound states, respectively.

Spiral-staircase arrangements have been observed in the crystal structures of the DNA-bound RecA-type helicases Rho and DnaB, as well as the AAA+ helicase E1, with translocation proposed to involve large-scale motions as subunits successively pass through the different conformational registers of the spiral<sup>27–29</sup>. Unexpectedly, the ATPase ring of the 26S proteasome in the substrate-engaged state displays a fixed spiral orientation with highly ordered densities (Fig. 7b). This is especially notable given that substrate stimulates the ATPase rate (Supplementary Fig. 2b) and that the enzyme was hydrolyzing at this stimulated rate when the sample was frozen for EM analysis. The vitrification within ~0.2 ms is fast enough to prevent thermally induced rearrangements and thus provides a true snapshot of the translocating proteasome. Although it is possible that substrate translocation is driven by only local motions of the pore loops in an otherwise fixed AAA+ spiral, it is more likely that the spiral is dynamic and the specific orientation that we observe in our structure represents a ‘dwell’ state adopted before or after coordinated ATP-hydrolysis events that rapidly progress around the ring. The uniform subunit interfaces formed between neighboring Rpts upon substrate engagement are consistent with this model, as they would facilitate such coordinated firing of subunits. A rapid progression of ATP hydrolysis-driven



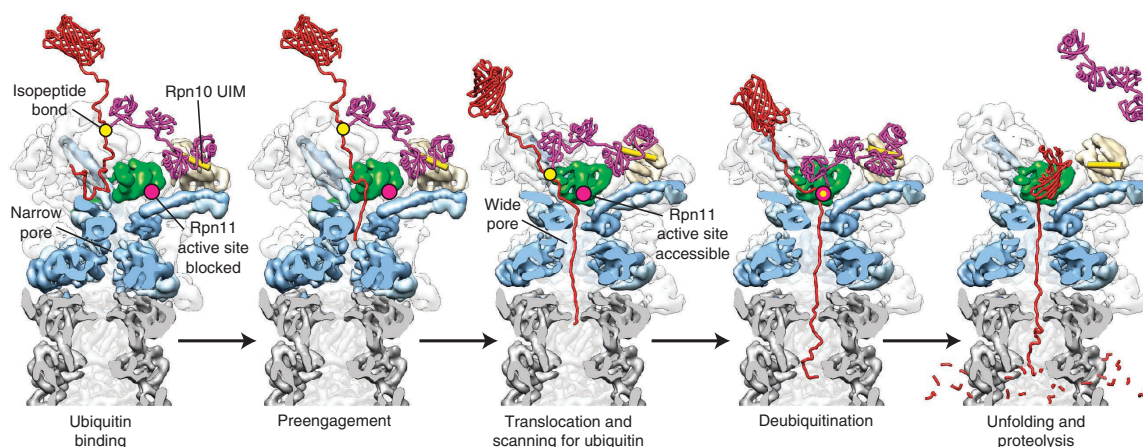


**Figure 8** Structure-based model for substrate engagement and degradation by the 26S proteasome. Cutaway side view of the proteasome reconstructions in the substrate-free and engaged conformations. In the first step, substrate (red) is tethered through its ubiquitin chain (purple) to the UIM of Rpn10 (yellow cylinder). In this preengaged state, the flexible substrate tail can enter the accessible N-ring pore and contact the uppermost subunits of the AAA+ domain spiral staircase. Upon substrate engagement, the Rpts become rearranged into a new spiral staircase with a widened central pore that is aligned with the N-ring and subjacent peptidase (gray). Concomitantly, Rpn11 (green) shifts to a central location directly above the N-ring pore, thus exposing its active site (pink dot) for ubiquitin scanning along the translocating polypeptide. All ubiquitin modifications are removed, as their isopeptide attachment site (yellow dot) passes by Rpn11, thus facilitating fast translocation, unfolding and degradation of the substrate.

conformational changes around the ring has been proposed for the AAA+ DNA packaging motor of the bacteriophage  $\phi 29$  (refs. 45,46). During translocation of a DNA substrate, this packaging motor spends 90% of its time in a stationary or dwell phase, during which ADP is released and subunits are loaded with ATP, and only 10% of its time in a 'burst' phase, during which substrate is translocated by coordinated conformational changes of subunits around the ring. A similar temporal distribution for the substrate-engaged proteasome, with 90% of particles in the dwell phase at any given time, would result in an EM reconstruction with an apparently fixed AAA+-ring spiral, as we observed. However, particles that are in the burst phase at the time of sample freezing may have caused the lower local resolution that we observed for the AAA+ ring in the substrate-bound compared to the preengaged structure (Supplementary Fig. 5a,b). The preengaged state may not exhibit a coordinated burst phase or undergo the same conformational changes associated with a rapid progressive hydrolysis around the ring because its individual subunits are not coupled by the uniform interfaces that are present in the substrate-engaged state.

The specific orientation of the translocation-competent spiral, with Rpt1 adopting the top position in all dwell-phase particles, probably originates from conformational constraints imposed by the heterohexameric architecture of the ATPase ring as well as its asymmetric surroundings. We propose that the Rpt ring adopts this spiral as soon as a substrate polypeptide is engaged in the central pore. Coordinated ATP hydrolysis then drives the tilting of individual AAA+ domains through the different subunit registers of the translocation-competent spiral, generating a power stroke that propels a certain length of polypeptide through the pore. After each stroke, the ring returns to the dwell-phase conformation with Rpt1 in the top position. Repeating this process thus drives the stepwise translocation of substrate into the peptidase. After the substrate has been completely translocated, the AAA+ ring, together with the rest of the regulatory particle, switches back to the preengaged conformation with a pronounced spiral staircase ready to accept the next incoming substrate.

## DISCUSSION

The work presented here provides the first insights, to our knowledge, into the structure of the actively translocating 26S proteasome

and outlines the transitions that accompany substrate engagement (Fig. 8 and Supplementary Movie 1). Notably, these new data help us to identify all previously described structures as representatives of a preengaged state with features that facilitate substrate engagement but are incompatible with further processing<sup>20–22,25,47</sup>. In this preengaged state, the entrance to the N ring is accessible to the unstructured initiation region of an incoming substrate whose ubiquitin chain is tethered to a proteasomal receptor. However, the central pore of the ATPase ring is constricted and not coaxially aligned with the subjacent peptidase. Furthermore, the DUB Rpn11 active site is occluded, and this prevents premature deubiquitination of the substrate before engagement by the ATPase ring. In this state, the AAA+ domains are arranged in a pronounced spiral staircase. Substrate interactions with Rpt subunits at the top of this spiral trigger the switching of the regulatory particle into a translocation-competent conformation that is characterized by a reorganized AAA+ ring with an alternative spiral arrangement, more uniform AAA-domain interfaces and a continuous central channel to the peptidase (Fig. 8). Rpn11 shifts to a central location directly above the N-ring pore, where its active site is accessible and ideally positioned to scan translocating polypeptides for ubiquitin chains and ensure complete deubiquitination. This substrate-engaged conformation of the regulatory particle is stabilized by an alternative set of lid-base interactions.

A similar proteasome conformation with a rearranged AAA+ ring and a continuous central channel has recently been observed in the presence of the slowly hydrolyzable ATP- $\gamma$ -S<sup>48</sup>, which we assume traps the ATPase motor in a dwell phase-like state. On the basis of these data and our substrate-bound structure of the 26S proteasome, we conclude that a spiral arrangement of ATPase subunits is functionally relevant for translocation. Our data are consistent with a mechanism in which a fast, highly coordinated wave of ATP hydrolysis-induced conformational changes around the ATPase ring propels the substrate through the central pore and into the peptidase. We propose that related AAA+ protein unfoldases operate by similar mechanisms, and in fact, recent single-molecule data for the unfoldase ClpX agree with this model of translocation (R. Maillard, K. Nyquist, M. Sen, C. Bustamante and A.M., unpublished data). Although future biophysical and biochemical studies will be necessary to describe the detailed mechanisms involved in proteasomal

engagement and translocation of substrate, the data presented here offer a structural framework for understanding these events.

## METHODS

Methods and any associated references are available in the [online version of the paper](#).

**Accession codes.** The cryo-EM density maps for the mutant 26S proteasomes (Rpn11<sup>AXA</sup> Rpn13Δ) in the absence and presence of substrate can be found at the Electron Microscopy Data Bank under accession numbers EMD-5668 and EMD-5669, respectively.

*Note: Supplementary information is available in the online version of the paper.*

## ACKNOWLEDGMENTS

We thank C. Boshore (University of California, Berkeley, Berkeley, California, USA) for providing the construct for the G3P model substrate. We thank E. Nogales for thoughtful discussions and for providing access to her EM facility. Finally, we thank the members of the Martin lab for helpful comments. M.E.M. acknowledges support from the American Cancer Society (grant 121453-PF-11-178-01-TBE), and G.C.L. is supported as a Damon Runyon Cancer Research Foundation Fellow (DRG 2055-10). This research was funded in part by the Searle Scholars Program (A.M.), start-up funds from the University of California Berkeley Molecular and Cell Biology Department (A.M.), the US National Institutes of Health (grant R01-GM094497-01A1 to A.M.), the US National Science Foundation CAREER Program (NSF-MCB-1150288 to A.M.) and the Lawrence Berkeley National Laboratory (G.C.L.).

## AUTHOR CONTRIBUTIONS

M.E.M. designed, expressed and purified proteasome constructs and performed biochemical experiments. G.C.L. performed the EM, processing and segmentation analyses. All authors contributed to experimental design, data analyses and manuscript preparation.

## COMPETING FINANCIAL INTERESTS

The authors declare no competing financial interests.

Reprints and permissions information is available online at <http://www.nature.com/reprints/index.html>.

- Finley, D. Recognition and processing of ubiquitin-protein conjugates by the proteasome. *Annu. Rev. Biochem.* **78**, 477–513 (2009).
- Sauer, R.T. & Baker, T.A. AAA+ proteases: ATP-fueled machines of protein destruction. *Annu. Rev. Biochem.* **80**, 587–612 (2011).
- Saeki, Y. & Tanaka, K. Assembly and function of the proteasome. *Methods Mol. Biol.* **832**, 315–337 (2012).
- Groll, M. *et al.* A gated channel into the proteasome core particle. *Nat. Struct. Mol. Biol.* **7**, 1062–1067 (2000).
- Thrower, J.S., Hoffman, L., Rechsteiner, M. & Pickart, C.M. Recognition of the polyubiquitin proteolytic signal. *EMBO J.* **19**, 94–102 (2000).
- Smith, D.M., Benaroudji, N. & Goldberg, A. Proteasomes and their associated ATPases: a destructive combination. *J. Struct. Biol.* **156**, 72–83 (2006).
- Glickman, M.H. *et al.* A subcomplex of the proteasome regulatory particle required for ubiquitin-conjugate degradation and related to the COP9-signalosome and eIF3. *Cell* **94**, 615–623 (1998).
- Glickman, M.H., Rubin, D.M., Fried, V.A. & Finley, D. The regulatory particle of the *Saccharomyces cerevisiae* proteasome. *Mol. Cell Biol.* **18**, 3149–3162 (1998).
- Tomko, R.J. Jr., Funakoshi, M., Schneider, K., Wang, J. & Hochstrasser, M. Heterohexameric ring arrangement of the eukaryotic proteasomal ATPases: implications for proteasome structure and assembly. *Mol. Cell* **38**, 393–403 (2010).
- Hamazaki, J. *et al.* A novel proteasome interacting protein recruits the deubiquitinating enzyme UCH37 to 26S proteasomes. *EMBO J.* **25**, 4524–4536 (2006).
- Leggett, D.S. *et al.* Multiple associated proteins regulate proteasome structure and function. *Mol. Cell* **10**, 495–507 (2002).
- Martin, A., Baker, T.A. & Sauer, R.T. Pore loops of the AAA+ ClpX machine grip substrates to drive translocation and unfolding. *Nat. Struct. Mol. Biol.* **15**, 1147–1151 (2008).
- Maillard, R.A. *et al.* ClpX(P) generates mechanical force to unfold and translocate its protein substrates. *Cell* **145**, 459–469 (2011).
- Aubin-Tam, M.E., Olivares, A.O., Sauer, R.T., Baker, T.A. & Lang, M.J. Single-molecule protein unfolding and translocation by an ATP-fueled proteolytic machine. *Cell* **145**, 257–267 (2011).
- Zhang, F. *et al.* Mechanism of substrate unfolding and translocation by the regulatory particle of the proteasome from *Methanocaldococcus jannaschii*. *Mol. Cell* **34**, 485–496 (2009).
- Erales, J., Hoyt, M.A., Troll, F. & Coffino, P. Functional asymmetries of proteasome translocase pore. *J. Biol. Chem.* **287**, 18535–18543 (2012).
- Zhang, F. *et al.* Structural insights into the regulatory particle of the proteasome from *Methanocaldococcus jannaschii*. *Mol. Cell* **34**, 473–484 (2009).
- Smith, D.M. *et al.* Docking of the proteasomal ATPases' carboxyl termini in the 20S proteasome's  $\alpha$  ring opens the gate for substrate entry. *Mol. Cell* **27**, 731–744 (2007).
- Rabl, J. *et al.* Mechanism of gate opening in the 20S proteasome by the proteasomal ATPases. *Mol. Cell* **30**, 360–368 (2008).
- Lander, G.C. *et al.* Complete subunit architecture of the proteasome regulatory particle. *Nature* **482**, 186–191 (2012).
- Bohn, S. *et al.* Structure of the 26S proteasome from *Schizosaccharomyces pombe* at subnanometer resolution. *Proc. Natl. Acad. Sci. USA* **107**, 20992–20997 (2010).
- Nickell, S. *et al.* Insights into the molecular architecture of the 26S proteasome. *Proc. Natl. Acad. Sci. USA* **106**, 11943–11947 (2009).
- Lasker, K. *et al.* Molecular architecture of the 26S proteasome holocomplex determined by an integrative approach. *Proc. Natl. Acad. Sci. USA* **109**, 1380–1387 (2012).
- Verma, R. *et al.* Role of Rpn11 metalloprotease in deubiquitination and degradation by the 26S proteasome. *Science* **298**, 611–615 (2002).
- Beck, F. *et al.* Near-atomic resolution structural model of the yeast 26S proteasome. *Proc. Natl. Acad. Sci. USA* **109**, 14870–14875 (2012).
- Yao, T. & Cohen, R.E. A cryptic protease couples deubiquitination and degradation by the proteasome. *Nature* **419**, 403–407 (2002).
- Thomsen, N.D. & Berger, J.M. Running in reverse: the structural basis for translocation polarity in hexameric helicases. *Cell* **139**, 523–534 (2009).
- Enemark, E.J. & Joshua-Tor, L. Mechanism of DNA translocation in a replicative hexameric helicase. *Nature* **442**, 270–275 (2006).
- Itsathitphisarn, O., Wing, R.A., Eliason, W.K., Wang, J. & Steitz, T.A. The hexameric helicase DnaB adopts a nonplanar conformation during translocation. *Cell* **151**, 267–277 (2012).
- Inobe, T., Fishbain, S., Prakash, S. & Matouschek, A. Defining the geometry of the two-component proteasome deproton. *Nat. Chem. Biol.* **7**, 161–167 (2011).
- Prakash, S., Tian, L., Ratliff, K.S., Lehotzky, R.E. & Matouschek, A. An unstructured initiation site is required for efficient proteasome-mediated degradation. *Nat. Struct. Mol. Biol.* **11**, 830–837 (2004).
- Martin, A., Baker, T.A. & Sauer, R.T. Protein unfolding by a AAA+ protease is dependent on ATP-hydrolysis rates and substrate energy landscapes. *Nat. Struct. Mol. Biol.* **15**, 139–145 (2008).
- Ortega, J., Lee, H.S., Maurizi, M.R. & Steven, A.C. Alternating translocation of protein substrates from both ends of ClpXP protease. *EMBO J.* **21**, 4938–4949 (2002).
- Chandra, A., Chen, L., Liang, H. & Madura, K. Proteasome assembly influences interaction with ubiquitinated proteins and shuttle factors. *J. Biol. Chem.* **285**, 8330–8339 (2010).
- Kim, Y.C., Li, X., Thompson, D. & Demartino, G.N. ATP-binding by proteasomal ATPases regulates cellular assembly and substrate-induced functions of the 26S proteasome. *J. Biol. Chem.* **288**, 3334–3345 (2012).
- Burton, R.E., Siddiqui, S.M., Kim, Y.I., Baker, T.A. & Sauer, R.T. Effects of protein stability and structure on substrate processing by the ClpXP unfolding and degradation machine. *EMBO J.* **20**, 3092–3100 (2001).
- Hwang, B.J., Woo, K.M., Goldberg, A.L. & Chung, C.H. Protease Pi, a new ATP-dependent protease in *Escherichia coli*, contains protein-activated ATPase and proteolytic functions in distinct subunits. *J. Biol. Chem.* **263**, 8727–8734 (1988).
- Janse, D.M., Crosas, B., Finley, D. & Church, G.M. Localization to the proteasome is sufficient for degradation. *J. Biol. Chem.* **279**, 21415–21420 (2004).
- Schneekloth, J.S. Jr. *et al.* Chemical genetic control of protein levels: selective *in vivo* targeted degradation. *J. Am. Chem. Soc.* **126**, 3748–3754 (2004).
- Zhang, M., Pickart, C.M. & Coffino, P. Determinants of proteasome recognition of ornithine decarboxylase, a ubiquitin-independent substrate. *EMBO J.* **22**, 1488–1496 (2003).
- Henderson, A., Erales, J., Hoyt, M.A. & Coffino, P. Dependence of proteasome processing rate on substrate unfolding. *J. Biol. Chem.* **286**, 17495–17502 (2011).
- Sato, Y. *et al.* Structural basis for specific cleavage of Lys 63-linked polyubiquitin chains. *Nature* **455**, 358–362 (2008).
- Glynn, S.E., Martin, A., Nager, A.R., Baker, T.A. & Sauer, R.T. Structures of asymmetric ClpX hexamers reveal nucleotide-dependent motions in a AAA+ protein-unfolding machine. *Cell* **139**, 744–756 (2009).
- Glynn, S.E., Nager, A.R., Baker, T.A. & Sauer, R.T. Dynamic and static components power unfolding in topologically closed rings of a AAA+ proteolytic machine. *Nat. Struct. Mol. Biol.* **19**, 616–622 (2012).
- Moffitt, J.R. *et al.* Intersubunit coordination in a homomeric ring ATPase. *Nature* **457**, 446–450 (2009).
- Chistol, G. *et al.* High degree of coordination and division of labor among subunits in a homomeric ring ATPase. *Cell* **151**, 1017–1028 (2012).
- da Fonseca, P.C., He, J. & Morris, E.P. Molecular model of the human 26S proteasome. *Mol. Cell* **46**, 54–66 (2012).
- Sledz, P. *et al.* Structure of the 26S proteasome with ATP- $\gamma$ S bound provides insights into the mechanism of nucleotide-dependent substrate translocation. *Proc. Natl. Acad. Sci. USA* **110**, 7264–7269 (2012).
- Pathare, G.R. *et al.* The proteasomal subunit Rpn6 is a molecular clamp holding the core and regulatory subcomplexes together. *Proc. Natl. Acad. Sci. USA* **109**, 149–154 (2012).

## ONLINE METHODS

**Yeast strain construction.** Genotypic information for every strain used in this study is provided in **Supplementary Table 1**. Wild-type proteasome holoenzyme was purified from the strain YYS40 (*MATa ade2-1 his3-11,15 leu2-3,112 trp1-1 ura3-1 can1-100 RPN11:RPN11-3XFLAG (HIS3)*)<sup>50</sup>. To generate the strain used to purify Rpn11<sup>AXA</sup> Rpn13 $\Delta$  holoenzyme, the *RPN11* promoter, coding sequence and terminator were cloned into pRS304 (*TRP1*). A 3 $\times$  Flag tag was inserted at the *RPN11* C terminus, and the two conserved active site histidines (defined by EXnHXHX10D) were mutated to alanines (H109A H111A). This plasmid was then integrated at the *TRP1* locus in the strain DOM90, thus resulting in a strain that contained both wild-type *RPN11* and a tagged *RPN11-AXA* mutant under control of its endogenous promoter. Rpn13 was deleted from this strain by integrating the KanMX6 sequence at the *RPN13* genomic locus, thus resulting in the strain  $\gamma$ AM11 (*MATa ade2-1 his3-11,15 leu2-3,112 ura3-1 can1-100 trp1-1::PRP11-rpn11AXA-3XFLAG-TRP1(pRS304) rpn13 $\Delta$ ::KanMX6*).

**Proteasome purification.** Wild-type and mutant proteasome was purified from *S. cerevisiae* essentially as described<sup>20</sup>. For holoenzyme purification, yeast cells from strains containing a 3 $\times$  Flag tag on Rpn11 were lysed by a SPEX Freezer/Mill (cat. no. 6870). Lysed cells were resuspended in lysis buffer containing 60 mM HEPES, pH 7.6, 50 mM NaCl, 50 mM KCl, 5 mM MgCl<sub>2</sub>, 0.5 mM EDTA, 10% glycerol, 0.2% NP-40 and an ATP-regeneration mix (5 mM ATP, 0.03 mg/ml creatine kinase and 16 mM creatine phosphate). Holoenzyme was bound to anti-Flag M2 affinity resin (Sigma) and washed with wash buffer (60 mM HEPES, pH 7.6, 50 mM NaCl, 50 mM KCl, 5 mM MgCl<sub>2</sub>, 0.5 mM EDTA, 10% glycerol, 0.1% NP-40 and 500 mM ATP) before elution with Flag peptide and separation by size-exclusion chromatography over Superose-6 in gel-filtration (GF) buffer (60 mM HEPES, pH 7.6, 50 mM NaCl, 50 mM KCl, 5 mM MgCl<sub>2</sub>, 0.5 mM EDTA and 500 mM ATP) containing 5% glycerol.

**Purification, ubiquitination and degradation of model substrates.** The GFP-titin-cyclin fusion substrate was purified by Ni-NTA affinity chromatography, then by size-exclusion chromatography as described<sup>20</sup>. The substrate (45  $\mu$ M) was modified with polyubiquitin chains by 45  $\mu$ M yeast Rsp5, 1  $\mu$ M yeast Uba1, 30  $\mu$ M yeast Ubc4 and 250  $\mu$ M ubiquitin (a 10:1 mixture of wild-type to methyl ubiquitin, to reduce the formation of very long ubiquitin chains). Degradation of the ubiquitinated GFP-fusion substrate by wild-type proteasome in GF buffer at 30 °C and in the presence of an ATP-regeneration system (5 mM ATP, 16 mM creatine phosphate and 6 mg/ml creatine phosphokinase) was monitored by the loss of fluorescence measured by a QuantaMaster spectrofluorimeter (PTI). The alternative substrate, consisting of the N1 domain of G3P fused to cyclin, was purified by Ni-NTA affinity followed by size-exclusion chromatography. This substrate (75  $\mu$ M) was ubiquitinated on its single lysine by 175 nM yeast Rsp5, 170 nM yeast Uba1, 5  $\mu$ M yeast Ubc4 and 1.2 mM ubiquitin (a 10:1 mixture of wild-type to methyl ubiquitin). Degradation was monitored by SDS-PAGE and Coomassie staining. This substrate was also labeled on an N-terminal cysteine with Cy5-maleimide (GE Healthcare, PA25031) for fluorescence visualization. Substrate was buffer-exchanged to remove reducing agent and incubated with Cy5-maleimide for 1 h at room temperature in the dark. The sample was then reduced with 10 mM DTT to neutralize excess dye and buffer-exchanged by a PD-10 column to remove free dye for subsequent ubiquitination. This substrate was imaged on a Typhoon Trio Variable Mode Imager (GE healthcare) with a 670-nm band-pass filter.

**ATP hydrolysis assay.** ATPase activity was quantified by an NADH-coupled ATPase assay. Proteasome holoenzyme (300 nM) was incubated with 1 $\times$  ATPase mix (3 U ml<sup>-1</sup> pyruvate kinase, 3 U ml<sup>-1</sup> lactate dehydrogenase, 1 mM NADH and 7.5 mM phosphoenol pyruvate) at 30 °C, in the presence or absence of 10  $\mu$ M ubiquitinated substrate. Absorbance at 340 nm was monitored for 900 s at 5-s intervals by a UV-vis spectrophotometer (Agilent).

**Cross-linking.** G3P substrate was either ubiquitinated or mock ubiquitinated by addition of all ubiquitination components except ubiquitin. Substrate was then dialyzed for 30 min into GF buffer to remove DTT, and the cysteine residue was activated for cross-linking by incubation with 1 mM 5,5'-dithiobis-(2-nitrobenzoic acid) (DTNB) for 5 min at room temperature. Substrate was then dialyzed again into GF buffer to remove free DTNB. Proteasomes containing Rpn11<sup>AXA</sup> and

HA-tagged Rpt1 with either a wild-type or cysteine-mutant pore loop (Rpt1 Y283C) (purified from  $\gamma$ AM12 and  $\gamma$ AM13, respectively) were buffer-exchanged to remove reducing agent. DTNB-activated substrate (~10  $\mu$ M) was then mixed with proteasome (~1  $\mu$ M) in the presence of an ATP-regeneration system, and substrate translocation and cross-linking were allowed to proceed for 30 min at 30 °C before the reaction was stopped by the addition of 200 mM iodoacetic acid. Samples were boiled after the addition of 2 $\times$  sample buffer and 5 M urea for separation by nonreducing SDS-PAGE. Rpt1 subunits with cross-linked substrate were detected by western blotting with an anti-HA antibody (12CA5, Santa Cruz Biotechnology, cat. no. sc-57592) at 1:10,000 dilution.

**Sample preparation for cryo-EM analysis.** Frozen-hydrated preservation of wild-type and Rpn11<sup>AXA</sup> Rpn13 $\Delta$  proteasome particles in the absence and presence of substrate was performed in a similar manner. In the case of wild type, 6  $\mu$ l of 8  $\mu$ M purified holoenzyme in GF buffer (60 mM HEPES, pH 7.6, 50 mM NaCl, 50 mM KCl, 5 mM MgCl<sub>2</sub>, 0.5 mM EDTA, 1 mM DTT and 0.5 mM ATP) with 2.5% glycerol was incubated with 15  $\mu$ l of 6  $\mu$ M ubiquitinated GFP-cyclin substrate that had been dialyzed against QAH buffer (20 mM HEPES, pH 7.6, 150 mM NaCl and 1 mM MgCl<sub>2</sub>). The holoenzyme and substrate were incubated at room temperature for 5 min, at which point excess unengaged substrate was depleted by the addition of 1  $\mu$ l of 2 $\times$  magnetic bead slurry (MagneHis Ni-Particles, Promega) and immediately plunge-frozen. The C-terminal His tag located at the end of the substrate's unstructured engagement regions would be blocked from interacting with the beads upon engagement by the proteasome, thus allowing depletion of only unengaged substrate. Purified Rpn11<sup>AXA</sup> Rpn13 $\Delta$  holoenzyme was diluted from a concentration of 18  $\mu$ M in GF with 5% glycerol to a concentration of 1.8  $\mu$ l in EM buffer (GF with 0.05% NP-40, 2 mM ATP and 0% glycerol). Diluted holoenzyme (38.8  $\mu$ l) was incubated with 1.3  $\mu$ l of 46  $\mu$ M G3P substrate in EM buffer for 5 min and immediately plunge-frozen.

All samples were plunge-frozen on 400-mesh C flats (Protochips Inc.) that contained 2- $\mu$ m holes with a spacing of 2  $\mu$ m and had been plasma-cleaned in a 75% argon/25% oxygen atmosphere at 15 W for 6 s by a Solarus plasma cleaner (Gatan, Inc). Aliquots (3  $\mu$ l) of the samples were applied to these hydrophilized grids, blotted for 3 s with Whatman no.1 filter paper and plunged into liquid ethane by a Vitrobot (FEI). The Vitrobot environment chamber was programmed to maintain a temperature of 4 °C and 100% humidity and to use a blotting offset of -1. Grids were stored in liquid nitrogen until being loaded into a Gatan 626 single-tilt cryo-transfer holder for data collection.

**Cryo-electron microscopy data collection and processing.** Frozen grids were inserted into a Tecnai F20 Twin transmission electron microscope operating at 120 keV, and data were collected on a Gatan 4,096  $\times$  4,096 CCD with the MSI-T application within the Legion automated EM package<sup>51</sup>. Wild-type proteasome particles in the presence of substrate were acquired at a nominal magnification of 80,000 $\times$  (1.45 Å per pixel at the specimen level), and all Rpn11<sup>AXA</sup> Rpn13 $\Delta$  were collected at 100,000 $\times$  (1.08 Å per pixel). All imaging used an electron dose of 20 e<sup>-</sup>/Å<sup>2</sup> with a randomly set focus ranging from -1.2 to -2.5  $\mu$ m. A total of 3,439, 4,740 and 5,328 micrographs were collected for the wild type + substrate, Rpn11<sup>AXA</sup> Rpn13 $\Delta$ , and Rpn11<sup>AXA</sup> Rpn13 $\Delta$  + substrate samples, respectively, with the MSI-T application of the Legion software<sup>51</sup>.

All preprocessing of data leading up to the three-dimensional reconstruction was performed within the Appion processing environment<sup>52</sup>. The contrast transfer function (CTF) of each micrograph was estimated with ACE2 concurrently with data collection. Forward projections of a previously solved proteasome structure<sup>20</sup> were used to generate templates for cross-correlation-based automated particle selection<sup>53</sup>. Carbon edges were masked out from the micrographs manually, and particles appearing within these regions were not considered for analysis. Micrographs that showed an 80% confidence in CTF estimation accuracy were extracted with a box size of 576 pixels for the wild-type data and 640 pixels for the Rpn11<sup>AXA</sup> Rpn13 $\Delta$  data. The resulting stacks of 98,632, 112,015 and 282,600 particles (for the wild type + substrate, Rpn11<sup>AXA</sup> Rpn13 $\Delta$ , and Rpn11<sup>AXA</sup> Rpn13 $\Delta$  + substrate, respectively) were each binned by a factor of two, and the particles were normalized to remove pixels whose values were above or below 4.5 $\sigma$  of the mean pixel value by XMIPP normalization<sup>54</sup>.

Each data set was processed independently, beginning with removal of false positives from automated particle selection, aggregates and singly capped particles. This was accomplished through two-dimensional classification using

several rounds of iterative multivariate statistical analysis (MSA) and multireference alignment (MRA) in IMAGIC<sup>55</sup>. Class averages depicting detailed views of doubly capped proteasomes were manually selected, and particles contributing to these views were used to generate a new stack. This new stack was subjected to MSA-MRA analysis, and again particles contributing to detailed class averages were separated into a new stack. Several rounds of classification in this manner resulted in a final stacks of 63,918, 80,011 and 188,400 particles for the wild type + substrate, Rpn11<sup>AXA</sup> Rpn13Δ, and Rpn11<sup>AXA</sup> Rpn13Δ + substrate, respectively. To inspect the conformational heterogeneity of the regulatory particles within these data sets, well-resolved class averages containing 200–400 particles depicting side views of the proteasome were selected, and the aligned particles contributing to each average were saved as an individual stack. Inspection of class averages calculated from the aligned particles for each stack showed that the regulatory particle of wild-type particles in the presence of substrate showed considerably more variability than did the Rpn11<sup>AXA</sup> Rpn13Δ particles (Supplementary Fig. 1a–c).

**Three-dimensional processing of the wild-type + substrate data set.** The conformational differences observed within the regulatory particle of the wild-type proteasome particles in the presence of substrate were not clear enough for correlation of distinct structural changes between the many holoenzyme orientations presented in the class averages, so projection-matching of the 1,000 class averages was used to arrive at an asymmetric model of the wild-type substrate-engaged proteasome. The previous wild-type reconstruction (EMDB-1992) was low-pass-filtered to 50-Å resolution and used as a starting model for five rounds of projection matching using EMAN2 and SPARX libraries, with forward projections generated at 15° increments. The resulting structure contained one regulatory particle reminiscent of the previously observed unbound state, whereas the other regulatory particle exhibited an altered organization (Supplementary Fig. 1d). This low-resolution model was then used as a starting point for projection matching of the full data set of 63,918 particles to yield an asymmetric 25-Å-resolution structure of the proteasome. This reconstruction showed with more detail the conformational differences between the regulatory particle, confirming that one particle remained in the previously observed unbound state while the other assumed an alternate conformation, presumably owing to interaction with substrate.

We next explored the possibility that this wild-type data set contained a mixture of substrate occupancy, in which some proteasome complexes were completely free of substrate and others contained substrate interactions at both regulatory particles. The asymmetric reconstruction was split into two densities through the center of the peptidase, and C2 symmetry was applied to each half holoenzyme (Supplementary Fig. 1d). The resulting substrate-free and doubly bound proteasome densities, along with the half-bound reconstruction, served as three seeds for multimodel projection matching using the full data set of wild-type particles with EMAN2 and SPARX libraries. No symmetry was enforced during this process to allow regression of the C2-symmetric initial models to a half-bound state in the case that such occupancies did not exist. At the conclusion of the refinement, the conformational organizations observed in the final densities reflected those of the three initial models, with 25,589 (40%), 22,367 (35%) and 15,962 (25%) of the particles as half bound, substrate free and doubly bound, respectively. Owing to a preservation of C2 symmetry in the substrate-free and doubly bound reconstructions, this symmetry was imposed during a final refinement of the particle alignments in FREALIGN<sup>56</sup>.

**Three-dimensional processing of the Rpn11<sup>AXA</sup> Rpn13Δ data sets.** Three-dimensional reconstructions of the substrate-free and substrate-engaged Rpn11<sup>AXA</sup> Rpn13Δ particle data sets were performed with EMAN2 and SPARX libraries, as described previously<sup>20</sup>. To minimize the introduction of model bias during the projection matching, the previously determined wild-type reconstruction (EMDB-1992) was low-pass-filtered to 50-Å resolution for use as a starting point for refinement of both data sets. A final refinement of the substrate-free and substrate-engaged particle alignments was performed in FREALIGN. C2 symmetry was enforced during all refinements, and the resolutions of the final reconstructions were estimated to be about 9 Å, on the basis of ‘gold-standard’ Fourier shell correlation calculations (cutoff at 0.143) from two independent refinements of half data sets<sup>57</sup>. A local resolution assessment of the reconstructions indicated that different components of the structures ranged in resolution

from 7 to 12 Å and were low-pass-filtered accordingly (Supplementary Fig. 5a,b). Local resolution calculations and localized low-pass filtering for all reconstructions were performed with the ‘bloccres’ and ‘bloccfil’ functions of the Bsoft package<sup>58</sup>. Notably, the addition of substrate appears to narrow the angular distribution of proteasome particles in vitreous ice (Supplementary Fig. 5c), and this provides a possible explanation for the unimproved resolution of the substrate-engaged data set relative to the substrate-free data set despite its containing substantially more particles.

To investigate the possibility that the conformation we observed for the substrate-engaged particles is in fact an alternative apo-state conformation, we reprocessed substrate-free wild-type and AXA-mutant particle data sets, using multimodel projection matching. The three models used for this refinement included a C2-symmetric proteasome containing two apo-state regulatory particles (EMDB-1992), a C2-symmetric proteasome containing two substrate-engaged regulatory particles (the substrate-engaged Rpn11<sup>AXA</sup> Rpn13Δ reconstruction) and an asymmetric proteasome containing one apo-state and one substrate-engaged regulatory particle. The three structures were low-pass-filtered to 15 Å so that the distinctive structural aspects that define each state could drive the separation of particles. These models contained a built-in control that would signify the presence of model bias during the reconstruction because the apo-state regulatory-particle density contained Rpn13, whereas the substrate-engaged state did not. At the end of the refinement, all wild-type reconstructions should contain Rpn13, regardless of state, and this subunit should be absent from all the mutant reconstructions. The same EMAN2/SPARX projection-matching algorithm that was used for the C2-symmetric reconstructions was used, although no symmetry was enforced, and particles were sorted into one of three input models. The three asymmetric back-projections were then used for the next round of projection matching and sorting.

Unexpectedly, a notable percentage of the proteasome particles from both data sets were classified to the model containing one apo-state and one substrate-engaged regulatory particle (the apo/substrate state). Of the substrate-free wild-type and mutant data sets, 29% and 46% contained proteasomes in this apo/substrate state, respectively. For each of these reconstructions, a globular density near the entrance to the ATPase pore accompanies the substrate-engaged regulatory particle, similar to the density attributed to GFP in the previously described wild-type reconstruction in the presence of substrate (Supplementary Fig. 5d). It is not possible that this density is a product of model bias, as the substrate-engaged mutant density used to generate the initial models did not contain this globular density, owing to the design of the substrate. The strict correlation between the appearance of this globular density and the rearranged proteasome conformation suggests that these regulatory particles were bound to endogenous substrate during the purification and freezing for imaging. Notably, there were insufficient fully substrate-engaged proteasomes (bound to both regulatory particles) in either data set to form a stable three-dimensional model during the refinement. From the initial set of apo wild-type particles, 69,485 and 28,321 particles contributed to the final back-projection of the apo and apo/substrate reconstructions, respectively. From the initial set of apo mutant AXA particles, 33,435 and 28,312 particles contributed to the final back-projection of the apo and apo/substrate reconstructions, respectively. The substrate-free subset of particles was extracted and reprocessed with C2 symmetry imposed to boost the signal-to-noise ratio and improve the overall resolution of the reconstruction.

The same methodology was used to determine the percentage of apo-state regulatory particles in the AXA mutant + substrate data set, but no such particles were found. 132,310 particles contributed to the final back-projection of the substrate-bound AXA mutant reconstruction. For all reconstructions described, low-resolution Fourier amplitudes of the final densities were dampened to match those of a generic protein in SPIDER<sup>59</sup>. On the basis of a previous segmentation of the subunits<sup>20</sup>, segmentation of the densities was performed manually with the volume tracer tool of UCSF Chimera<sup>60</sup>.

50. Sone, T., Saeki, Y., Toh-e, A. & Yokosawa, H. Sem1p is a novel subunit of the 26 S proteasome from *Saccharomyces cerevisiae*. *J. Biol. Chem.* **279**, 28807–28816 (2004).

51. Suloway, C. *et al.* Automated molecular microscopy: the new Legion system. *J. Struct. Biol.* **151**, 41–60 (2005).

52. Lander, G.C. *et al.* Appion: an integrated, database-driven pipeline to facilitate EM image processing. *J. Struct. Biol.* **166**, 95–102 (2009).

53. Roseman, A.M. FindEM: a fast, efficient program for automatic selection of particles from electron micrographs. *J. Struct. Biol.* **145**, 91–99 (2004).
54. Sorzano, C.O. *et al.* XMIPP: a new generation of an open-source image processing package for electron microscopy. *J. Struct. Biol.* **148**, 194–204 (2004).
55. van Heel, M., Harauz, G., Orlova, E.V., Schmidt, R. & Schatz, M. A new generation of the IMAGIC image processing system. *J. Struct. Biol.* **116**, 17–24 (1996).
56. Grigorieff, N. FREALIGN: high-resolution refinement of single particle structures. *J. Struct. Biol.* **157**, 117–125 (2007).
57. Scheres, S.H. & Chen, S. Prevention of overfitting in cryo-EM structure determination. *Nat. Methods* **9**, 853–854 (2012).
58. Heymann, J.B. & Belnap, D.M. Bsoft: image processing and molecular modeling for electron microscopy. *J. Struct. Biol.* **157**, 3–18 (2007).
59. Frank, J. *et al.* SPIDER and WEB: processing and visualization of images in 3D electron microscopy and related fields. *J. Struct. Biol.* **116**, 190–199 (1996).
60. Goddard, T.D., Huang, C.C. & Ferrin, T.E. Visualizing density maps with UCSF Chimera. *J. Struct. Biol.* **157**, 281–287 (2007).